Type: Regular article

Title: Syndromic features and mild cognitive impairment in mice with genetic reduction on p300 activity: Differential contribution of p300 and CBP to Rubinstein-Taybi syndrome etiology

Authors and author addresses: [1] Jose Viosca, [1] Jose P. Lopez-Atalaya, [1] Roman Olivares, [2] Richard Eckner and [1] Angel Barco

[1] Instituto de Neurociencias de Alicante (Universidad Miguel Hernández-Consejo Superior de Investigaciones Científicas). Campus de Sant Joan. Apt. 18. Sant Joan d'Alacant. 03550. Alicante, Spain

[2] Department of Cell Biology & Molecular Medicine. UMDNJ. New Jersey Medical School. 185 South Orange Ave. Newark, NJ 07101

Corresponding author: Angel Barco, Instituto de Neurociencias de Alicante (Universidad Miguel Hernández – Consejo Superior de Investigaciones Científicas), Campus de Sant Joan, Apt. 18, Sant Joan d'Alacant 03550, Alicante, Spain. Tel: +34 965 919232. Fax: +34 965 919492. Email: abarco@umh.es

ABSTRACT

Rubinstein-Taybi syndrome (RSTS) is a complex autosomal-dominant disease characterized by mental and growth retardation and skeletal abnormalities. A majority of the individuals diagnosed with RSTS carry heterozygous mutation in the gene *CREBBP*, but a small percentage of cases are caused by mutations in *EP300*. To investigate the contribution of p300 to RSTS pathoetiology, we carried out a comprehensive and multidisciplinary characterization of $p300^{+/-}$ mice. These mice exhibited facial abnormalities and impaired growth, two traits associated to RSTS in humans. We also observed abnormal gait, reduced swimming speed, enhanced anxiety in the elevated plus maze, and mild cognitive impairment during the transfer task in the water maze. These analyses demonstrate that $p300^{+/-}$ mice exhibit phenotypes that are reminiscent of neurological traits observed in RSTS patients, but their comparison with previous studies on CBP deficient strains also indicate that, in agreement with the most recent findings in human patients, the activity of p300 in cognition is likely less relevant or more susceptible to compensation than the activity of CBP.

Keywords: Mental retardation; Rubinstein-Taybi syndrome; histone acetyltransferase; learning and memory; mouse model

Introduction

Rubinstein-Taybi syndrome (RSTS, OMIM #180849) is a complex autosomal-dominant disease characterized by mental impairment, growth retardation and characteristic skeletal abnormalities, such as apparent hypertelorism, prominent nose, malpositioned ears and broad thumbs and toes (Rubinstein and Taybi, 1963). Petrij and colleagues discovered fourteen years ago that about 40% of the individuals diagnosed with RSTS carried heterozygous mutations in *CREBBP*, the gene encoding for the CREB binding protein (CBP) (Petrij et al., 1995). Later studies have increased this number up to 60% of the individual diagnosed with this condition (Bentivegna et al., 2006), and revealed that a small percentage (~3%) of cases diagnosed as RSTS were caused by mutations of the gene *EP300*, which encodes for the co-activator p300 that is highly homologous to CBP (Bartholdi et al., 2007; Roelfsema et al., 2005; Zimmermann et al., 2007).

CBP and p300 proteins function as co-factors for many transcription factors (Chan and La Thangue, 2001) including several transcription factors known to be regulated or induced by neuronal activity, such as CREB, c-Fos, c-Jun, or NF-κβ. In addition, both proteins have histone acetyltransferase (HAT) activity that targets the N-terminal unstructured tails of histones and may contribute to transcriptional activation by relaxing the structure of the nucleosomes (Ogryzko et al., 1996). Their role in activity-dependent chromatin modification and gene expression may account for at least part of the cognitive and physiological alterations associated to mental retardation in RSTS patients.

Although the primary sequence of p300 and CBP are more than 70% similar and they have many common interaction partners, these two proteins have distinct cellular

functions and cannot always replace one another (Kalkhoven, 2004). The recent characterization of a number of mouse strains deficient in CBP activity has provided important new insight into the role of CBP in RSTS molecular etiology and opened new therapeutic avenues to treat this condition (Alarcon et al., 2004; Bourtchouladze et al., 2003; Korzus et al., 2004; Wood et al., 2006; Wood et al., 2005; reviewed in Barco, 2007). In contrast, the role of p300 in cognition and behavior remains poorly explored, although it has been recently shown that conditional transgenic mice expressing an inhibitory truncated form of p300 had mild memory deficits (Oliveira et al., 2007).

Here, we carried out a comprehensive analysis, including anatomical, behavioral, biochemical and gene profiling assays, of mice bearing a deleted p300 allele. Our results demonstrate skeletal abnormalities reminiscent of RSTS, mild motor and cognitive deficits and enhanced anxiety in the elevated plus maze, but unaltered levels of acetylated histones and negligible changes in gene expression except for *p300* itself. In agreement with recent conclusions of studies in human patients, the comparison of the behavioral phenotypes of *cbp* and *p300* mutants indicates that CBP, as compared to p300, plays a major role in cognitive abilities.

Materials and Methods

Animals

The generation of cb$p^{+/-}$ (Tanaka et al., 1997) and $p300^{+/-}$ (Yao et al., 1998) mice has been described before. CBP deficient mice were maintained in a mixed genetic background (F2 of C57BL/6J and DBA) because they cannot be maintained into a pure C57BL/6J background (Alarcon et al., 2004). P300 deficient mice were maintained in a

C57BL/6J pure background at least otherwise is indicated. Mice were group housed in single-sex cages on a light:dark cycle (12/12 h) with food and water available *ad libitum*. The wild type mice used as control were, in all cases, littermates of the mutant mice. Mice were maintained according to animal care standards established by the European Union and all the protocols were approved by the Institutional Animal Care and Use Committee.

Behavior

For all behavioral tasks, we used adult male mutant and control littermates in a C57BL/6J pure background. The experimenter was blind to genotypes. The result of the PCR-based genotyping was provided as a factor for statistical analysis of the behavioral data once the battery of tasks was concluded. *SHIRPA primary screen.* Mice were conducted using a modification of Irwin procedure (Irwin, 1968) as previously described (Rogers et al., 1997; Viosca et al., 2008). Statistical analyses used t-tests and Mann Whitney tests. *Open field:* Mice were placed in 50×50 cm^2 open-field chambers (170 lux on the floor) and monitored throughout the test session (30 min) by a video-tracking system (SMART, Panlab S.L., Barcelona), which monitors up to four animals simultaneously and records the position of each animal every 0.5 sec. Data were analyzed with repeated measures ANOVA with "genotype" as the between subject factor and "time bin" as the repeated factor. *Anxiety Test:* Mice were placed in the center of the elevated plus maze and their behavior was recorded for 5 min with a camera located above the maze using SMART software. Time spent and number of entries in the different compartments (closed and open arms) were assessed. Lighting levels were 210 lux in the open arms and 45 lux in the closed arms. Data were analyzed using t-test. *Rotarod:* Mice were first trained on a

rotarod (PanLab, S.L, Barcelona) at a constant speed (~4 rpm). Mice received three trials per day for three days. A steady level of performance was attained in both genotypes. On the testing day, the rotarod was set to increase 1 rpm every 30 sec starting at 4 rpm and the interval for mice to fall off was measured. T-test was used for statistical analysis. *Object recognition:* This task was performed as previously described (Viosca et al., 2008), with a 15 minutes training session and a 15 minutes testing session 24 h after training. The use of different objects as novel or familiar, as well as the relative position of the novel object, was balanced between genotypes. Exploration times during training were analyzed using a repeated measures ANOVA including "genotype" and "training object" as between subject factors and "object location" as the repeated factor. Exploration times during testing were analyzed using a repeated measures ANOVA including "genotype" and "training object" as between subject factors and "object" (new vs old) as the repeated factor. *Water Maze:* The task was performed as previously described (Viosca et al., 2008). The experiment was divided in three phases: three days of visible platform task (V1-V3), eight days of hidden platform task (H1-H8), and five days of transfer task (T1-T5) in which the hidden platform was moved to the opposite corner. To evaluate the retention of the previously acquired information, three probe trials (P1-P3, indicated by arrows in Figure 3) of 60 sec duration, in which the platform was removed, were performed 24 h after session H4, H8 and T5. Four trials, 120 s maximum and 30-60 min ITI (inter-trial interval) were given daily. For each session, the scores of the four trials were averaged for each individual. Path length, time in walls and swim speed were analyzed using Repeated measures ANOVAs including "genotype" as the between subject factor and "session" as the repeated factor. For the analysis of probe

trials, we calculated quadrant occupancy (% of time) and the number of crossings in an annulus (area double than platform) located at platform position (TQ, target quadrant) and at equivalent positions in the other three quadrants of the pool. T-tests and Repeated measures ANOVAs including "genotype" as the between subject factor and "quadrant" as the repeated factor were used for their analysis. *Fear conditioning:* On training day, the mice were placed in the conditioning chamber (Panlab S.L., Barcelona, Spain) for 2 min before the onset of a tone at 2800 Hz, 85 dB (conditioned stimulus, CS), which lasted for 30 s. The last 2 s of the CS were paired with a 0.7 mA foot shock (unconditioned stimulus, US). After an additional 30 s in the chamber, mice were returned to their home cage. Conditioning was assessed 24 h later by scoring freezing behavior using a piezoelectric accelerometer that transduced animal movements. The software (*Freezing* from Panlab S.L., Barcelona, Spain) was configured to consider an interval longer than 2 sec in which the signal remained below a given threshold as a freezing episode. Testing occurred first in the context in which mice were trained (contextual fear conditioning) and three hours later in a novel environment in which, after a 1 min of habituation, the same tone that was presented during training was given during 120 s (cued fear conditioning).

CT scan

CT acquisition was performed with an ARGUS PET/CT (SUINSA Medical Systems, S.A., Madrid, Spain), using an amperage of 150 mA and a voltage of 45 kV. Mice were anesthetized with inhaled isofluorane (5% for induction, 2% for maintenance) during acquisition. Raw images were reconstructed using FDK algorithm with a voxel size of

0.25 x 0.25 x 0.25 mm^3. Mid sagittal skull planes from wild type and mutant mice were aligned and compared using MHWKS (GE Healthcare, Chalfont St. Giles, UK) software.

Western blot and histological techniques

Nissl staining, hippocampal protein extracts and Western blot analysis were carried out as previously described (Alarcon et al., 2004). Antibodies recognizing total levels of histones H2B and H3 were obtained from Upstate (Charlottesville, USA) and Abcam (Cambridge, UK) respectively. The different acetyl-histone antibodies, specific for the panacetylated forms of H2A (K5, K9), H2B (K5, K12, K15, K20), H3 (K9, K14) and H4 (K5, K8, K12, K16), were produced in our laboratory. Western Blot results were statistically analyzed using t-tests. For immunohistochemistry, mice were anesthetized with a mix of ketamine and xylazine, perfused with 4% paraformaldehyde and postfixed overnight. 50 µm sections were obtained using a vibratome and stained as described (Lopez de Armentia et al., 2007). Antibodies against MAP2 and Synaptophysin were obtained from Sigma-Aldrich Química S.A. (Barcelona, Spain). As controls for the detection of changes in the acetylation of neuronal histones, we used protein samples and brain sections from mice intraperitoneally injected with sodium butyrate at a dose of 1.2 g/kg and sacrificed 30 min after injection.

Microarray analysis and quantitative RT-PCR

We obtained triplicate samples containing total RNA from the hippocampi of four 3-month old females of either genotype (in total 12 *p300*$^{+/-}$ mice and 12 wild type littermates were used in the experiment). Mouse Genome 430 2.0 genechips were hybridized, stained, washed and screened for quality according to the manufacturer's protocol. The microarray data was normalized and statistically analyzed using

GeneSpring GX (Agilent Technologies, Santa Clara, CA). The list of significantly changed probe sets shown in Supplemental Table 1 was obtained after filtering by signal intensities (20-100th percentile in the raw data), statistical significance (P<0.05) and fold change (>1.5). Parametric and non-parametric tests rendered similar results. This dataset will be accessible at the GEO database upon acceptance of the manuscript. qRT-PCR was carried out in an Applied Biosystems 7300 real-time PCR unit using *SYBR GreenER qPCR supermix* (Invitrogen, Carlsbad, CA) and primers specific for p300, CBP, GAPDH and the other genes show in Figure 6. Each independent sample was assayed in duplicate and normalized using GAPDH levels.

Results

Facial dysmorphia and other syndromic features in p300 deficient mice

Although preliminary studies indicated that mice bearing an inactive *p300* allele did not show any gross skeletal malformation during development (Yao et al., 1998), we observed that a large percentage of adult *p300*$^{+/-}$ mice (~75%) presented facial dysmorphia characterized by a prominent forehead and blunt nose (Figure 1A). This observation was confirmed using computerized tomography (CT) analysis, which revealed normal cranial length and width, but shortened and depressed nasal bridge in *p300*$^{+/-}$ mice (Figure 1B, left). For comparison purposes, we also performed CT scans of *cbp*$^{+/-}$ mice, which also confirmed the pronounced facial dysmorphia phenotype (Figure 1B, right).

P*300*$^{+/-}$ mice also showed other syndrome-related features like postnatal growth. Thus, adult *p300*$^{+/-}$ mice exhibited reduced body weight (Figure 1C: wt=28.6±0.8 g, *p300*$^{+/-}$=24.9±0.5 g, t_{44}=3.598, p=0.001) and length (Figure 1C: wt=87.7±1.0 mm, *p300*$^{+/-}$

=83.9±0.7 mm, t_{28}=2.749, p=0.010). Despite the marked alteration of skull morphology, Nissl staining and immunohistochemistry of brain sections using the neuronal markers MAP2 and synaptophysin did not reveal gross abnormality in the brain of *p300*$^{+/-}$ mice (Figure 2).

Interaction of phenotype with genetic background

In the proceeding of these experiments, we observed a reduced transmission of the p300 mutant allele (Table 1: p<0.001, Fisher's exact test). We were able to rescue this phenotype by transferring the mutation from a pure C57BL/6J genetic background to a mixed genetic background (50% DBA, 50% C57BL6/J), in which the expected mendelian ratio was observed (Table 1). Interestingly, previous studies on c*bp*$^{+/-}$ mice had also revealed the interaction of CBP deficiency with the genetic background (Alarcon et al., 2004). Mice maintained in the mixed phenotype still exhibited facial dysmorphia, although milder than in the pure background, and impaired postnatal growth (Figure 1D: weight: wt=32.1±0.6 g, *p300*$^{+/-}$=28.3±0.5 g, t_{37}=4.053, p<0.001; length: wt=105.8±2.6 mm, *p300*$^{+/-}$=97.8±2.0 mm, t_{14}=2.428, p=0.029). These results support an interaction between genetic background and the expression of p300 deficiency.

Neurological examination, emotivity and exploratory behavior in p300$^{+/-}$ *mice*

We carried out a comprehensive behavioral analysis of *p300*$^{+/-}$ mice aimed to model some of the neurological traits observed in RSTS patients. First, we subjected *p300*$^{+/-}$ mice to a battery of basal neurological tests. No differences were observed between *p300*$^{+/-}$ mice and control siblings in basic reflexes, strength, muscle tone and many other

parameters evaluated in this primary screen (Table 2). However, mutant mice exhibited low pelvic elevation during ambulation (Figure 3A: wt=1 out of 11 animals (9%), *p300*$^{+/-}$ =6 out of 10 animals (60%); p=0.024, Fisher´s exact test). We also examined the performance of *p300*$^{+/-}$ mice in an accelerated paradigm for the RotaRod, a test of motor coordination and learning, and we did not find significant difference between genotypes (Figure 3B, wt=210.2±28.6 sec, *p300*$^{+/-}$=247.2±28.8 sec, 5 wt and 8 mutants, t_{11}=-0.856, p=0.410).

We next examined the behavior of *p300*$^{+/-}$ mice in an open field, a test for basic locomotor and exploratory behavior. Mutant mice showed normal exploratory activity as assayed by ambulatory distance, walking speed and other parameters (Figure 3C: $F_{(1,19)\ genotype}$=2.039, p=0.170; $F_{(5,95)\ bin\ x\ genotype}$=0.510, p=0.768; and results not shown). We found no differences between mutant mice and their wild type siblings in the time spent in the center of the arena, a common measure of anxiety (Figure 3D: $F_{(1,19)\ genotype}$=0.535, p=0.473; $F_{(5,95)\ bin\ x\ genotype}$=0.300, p=0.912). We also studied these mice in the elevated plus maze, a task where mice face a conflict between their tendency to explore new environments and their innate aversion to open, brightly light spaces. Mutant mice showed a reduced number of arm entries (Figure 3E: t_{18}=3.306, p=0.004) and spent less amount of time in the open arms (Figure 3F: t_{18}=2.324, p=0.032), suggesting enhanced anxiety in *p300*$^{+/-}$ mice.

Cognitive abilities in p300$^{+/-}$ *mice*

We next examined the performance of *p300*$^{+/-}$ mice in a battery of cognitive tasks to assess whether a reduced level of p300 effected learning and long-term memory

formation. *P300*$^{+/-}$ mice were first evaluated in a novel object recognition task, a non aversive memory task that relies on the natural exploratory behavior of mice. During training, both genotypes spent similar time exploring the objects and did not show a preference for either one of the identical objects. During testing, both mutant and wild-type littermates spent more time exploring the novel object (Figure 4A: $F_{(1,12)\ object}$= 9.790, p=0.009), without differences between genotypes ($F_{(1,12)\ genotype\ x\ object}$= 0.646, p=0.437) indicating a similar 24 h recognition memory for the old object.

We then examined the performance of *p300*$^{+/-}$ mice in spatial navigation using the Morris water maze. We divided the experiment in three phases: (a) the visible platform task (3 days) to evaluate vision, motivation and swimming performance, (b) the hidden platform task (8 days) to examine spatial learning, and (c) the transfer task (5 days), in which the hidden platform was relocated in a different quadrant, to examine learning flexibility. We assessed spatial memory performing probe trials on days 5 and 9 of the hidden platform task and day 6 of the transfer task. During training in the visible platform task, mutant mice and control siblings did not differ in escape path length or latency (Figure 4B: $F_{(1,19)\ genotype}$=1.880, p=0.186, $F_{(2,38)\ genotype\ x\ session}$=1.414, p=0.256; and results not shown). In agreement with our observations in the elevated plus maze, mutant mice showed more thigmotaxis, an indication of enhanced anxiety (Figure 4C: $F_{(1,19)\ genotype}$=8.029, p=0.011; $F_{(2,38)\ genotype\ x\ session}$=0.178, p=0.837). Interestingly, p300 deficient mice, like CBP deficient mice (Alarcon et al., 2004), swam slower than their control littermates during the visible platform task (Figure 4D: $F_{(1,19)\ genotype}$=5.636, p=0.028; $F_{(2,38)\ genotype\ x\ session}$=0.018, p=0.982). The same trend toward reduced swimming speed was also observed during training in the hidden platform task (Figure 4D: $F_{(1,19)}$

$_{genotype}$=3.967, p=0.061; $F_{(7,133)\ genotype\ x\ session}$=0.783, p=0.387). In contrast, we did not longer observe enhanced thigmotaxis (Figure 4C: Hidden: $F_{(1,19)\ genotype}$=0.338, p=0.568; Transfer: $F_{(1,19)\ genotype}$=1.746, p=0.202). *P300*$^{+/-}$ mice performed as well as control siblings both in escape latency and path length indicating normal spatial learning. The probe trials carried out on day H5 and 24 h after H8 did not reveal significant differences between genotypes (Figure 4E and Supplemental Figure S1A-B). In contrast, we found that *p300*$^{+/-}$ mice showed a significant delay in learning the new platform position in the transfer task (Figure 4B: from T2 to T5, $F_{(1,19)\ genotype}$=5.552, p=0.029). In fact, *p300*$^{+/-}$ mice spent significantly more time in the quadrant of the pool were the platform was originally located (Figure 4F: from T2 to T5, $F_{(1,19)\ genotype}$=5.058, p=0.037), suggesting that *p300*$^{+/-}$ mice could be less flexible than their control littermates. This initial deficit in the transfer task was overcome with further training and *p300*$^{+/-}$ mice and control siblings performed equally well a third probe trial (Figure 4G: wt=54±2%, *p300*$^{+/-}$=47±6%, p=0.285; and Supplemental Figure S1C), indicating that mutant mice were able to learn the new platform location.

We concluded our behavioral analysis examining two forms of associative memory: contextual and cued fear conditioning. These tasks measure the capability of the mouse to form an association between an aversive stimulus (mild foot shock) and neutral environmental cues (context) or a tone (cued). We did not observe any significant difference between genotypes neither during training nor testing (Figure 4H).

Chromatin acetylation in p300$^{+/-}$ *mice*

We have previously reported that *cbp*$^{+/-}$ mice had a specific deficit in histone H2B acetylation (Alarcon et al., 2004), whereas a recent study showed that transgenic mice expressing a truncated form of p300, p300Δ, had a mild reduction in the acetylation level of histone H3 in the hippocampus (Oliveira et al., 2007). We investigated the acetylation state of all four core histones in bulk chromatin of hippocampal tissue in p300 deficient mice and control siblings (Figures 5A-B). We did not observe any significant change in the global level of acetylation of histones H2A, H2B, H3 and H4 in the hippocampus of *p300*$^{+/-}$ mice (Figure 5B, top: total H2B, p=0.659; total H3, p=0.990; AcH2A, p=0.717; AcH2B, p=0.600; AcH3, p=0.427; AcH4, p= 0.910; n=3 per genotype). Hippocampal samples of *cbp*$^{+/-}$ mice, in which we confirmed the specific deficit in histone H2B acetylation (Figures 5A-B, p=0.003, n=4 per genotype), as well as hippocampal extracts from wild type mice treated with the inhibitor of histone deacetylases (HDACi) sodium butyrate and displaying histone hyperacetylation (Figure 5A), were included as controls in this analysis. To confirm the negative result in *p300*$^{+/-}$ mice and extend our analysis to other brain regions, we immunostained sagittal brain sections of *p300*$^{+/-}$ and wild type mice with antibodies against different acetylated histones. No difference between genotypes was detected although our technique revealed a dramatic increase in the acetylation level of the four histones by sodium butyrate (Figure 5C).

Gene profiling in the hippocampus of p300$^{+/-}$ *mice*

More than 10% of known transcription factors have been shown to interact with the coactivators CBP and p300. In fact, p300 exhibits one of the largest connectivity found in interactome analyses (Kasper et al., 2006). Therefore, it would not be surprising that the

loss or reduction of p300 caused broad and dramatic alterations in gene expression. To identify those genes whose expression was altered in the hippocampus of p300 deficient mutants, we performed a gene profiling analysis of hippocampal tissue using high-density oligonucleotide microarrays. Unexpectedly, we found that *p300* heterozygous mice did not show dramatic changes in gene expression. Statistical filtering revealed very few significant changes and fold changes were never larger than 2. In fact, only 16 probe sets showed a significant fold change larger than 1.5 (Supplementary Table 1). Moreover, most of these weak changes could not be validated by quantitative real-time RT-PCR analysis (Figure 6). Importantly, this list included the probe set targeted to p300 transcripts, whose downregulation was confirmed by qRT-PCR ($p<0.001$). We did not find significant changes in the expression of *cbp* neither in the microarray nor in the qRT-PCR analyses (Figure 6; $p= 0.613$), indicating that p300 deficiency does not cause the compensatory upregulation of its paralogous gene.

Discussion

We carried out a comprehensive neurological characterization of adult $p300^{+/-}$ mice. We did not observe gross neuroanatomical changes or alterations in histone acetylation or gene expression. Our analysis, however, revealed impaired growth and facial dysmorphia, two traits associated to RSTS in humans. We also observed abnormal gait, reduced swimming speed, enhanced anxiety in the elevated plus maze, and mild cognitive impairment during the transfer task in the water maze. Behavioral studies of individuals suffering from RSTS have revealed poor coordination and impaired learning of motor skills, as well as short attention span, stubbornness, sudden mood changes during early

adulthood and anxiety-related behaviors, such as the obsessive-compulsive disorder described in some patients (Hennekam et al., 1992; Levitas and Reid, 1998). Some of the phenotypes detected in *p300*$^{+/-}$ mice are therefore reminiscent of neurological traits observed in RSTS patients.

Previous studies on p300 deficient mice were limited to the assessment of motor performance at the rotarod in mice bearing homozygous mutations in the KIX domain (Oliveira et al., 2006), which revealed no phenotype, and the evaluation of hippocampus-dependent memory in transgenic mice expressing a putative dominant negative p300 variant (Oliveira et al., 2007). Our analysis extends these studies both in its scope, we examined *p300*$^{+/-}$ mice in a comprehensive battery of behavioral tasks and performed additional assays, such as CT and microarray analyses, as well as in its potential to model RSTS pathoetiology since the genetic mutation in the strain investigated here, a deletion of exons 4-6 (Yao et al., 1998), resembles the situation of 3 out of 6 identified RSTS patients bearing mutations on *EP300* (Foley et al., 2009; Roelfsema and Peters, 2007) (Table 4). Previous studies in homozygous mice have provided compelling evidence of the effects of this mutation in mouse physiology, including early embryonic lethality (Phan et al., 2005; Yao et al., 1998). Despite the dramatic effects of the mutation in homozygosis, the analysis of heterozygous mice revealed relatively modest neurological deficits and a strikingly small impact on gene expression. Other than the expected reduction in the level of p300 messenger, we could not confirm additional changes in hippocampal gene expression. The absence of changes in CBP expression, both in adult *p300*$^{+/-}$ mice (Figure 5D) and in *p300*$^{+/-}$ and *p300*$^{-/-}$ embryos (Yao et al., 1998) discards that the compensatory upregulation of its paralogous gene underlays the relatively modest

impact of p300 deficiency. The comparison of CBP and p300 deficient mice in other areas of research has revealed that these two coactivators play distinct functions in myogenesis (Roth et al., 2003) and T-cell development (Kasper et al., 2006). The comparison of the results presented here with those previously shown for CBP deficient mice suggest that CBP and p300 also play unique roles in the nervous system.

Recent studies on RSTS patients have revealed that the mutations in the *EP300* locus are twenty times less frequent than in *CREBBP* locus. Although classical RSTS facial features and some skeletal malformation were observed in the six patients with mutations in the *EP300* locus identified so far, none of them showed the classical malformations both on hands and feet that were originally considered mandatory for the diagnosis of RSTS (Bartholdi et al., 2007; Foley et al., 2009). Mental impairment in patients bearing mutations in *EP300* also seems to be milder than in the average *CREBBP* patient (Bartholdi et al., 2007; Foley et al., 2009; Zimmermann et al., 2007). In fact, it has been suggested that most *EP300* mutations could be underdiagnosed or associated with other phenotypes, instead of classical RSTS (Zimmermann et al., 2007). This underdiagnosis could be due to the fact that the mutation at the *EP300* locus does not necessarily develop an observable RSTS condition because of individual differences in the expression of compensatory factors. This view is consistent with our results in mouse models showing that the reduction of p300 activity, although associated to postnatal growth impairment and some other syndromic traits, had milder effects in cognition than a similar reduction of CBP activity, and with our observation that genetic background influenced the viability and the strength of some phenotypes in $p300^{+/-}$ mice. This comparison highlights the specificity and relevance of the HAT activity of CBP in

cognition and neuronal plasticity revealed in previous studies (Alarcon et al., 2004; Korzus et al., 2004; Wood et al., 2005).

Acknowledgments

The authors thank Manuel Desco and Francisca Mulero for their help in the acquisition and analysis of CT data and Maria Jimenez-Minchan for excellence technical assistance in histological preparations. We also thank Luis M. Valor and Lidia Larizza for critical reading of the manuscript and for helpful comments. This work was supported by the European Commission grant MEXT-CT-2003-509550, the Spanish Ministry of Science and Innovation Grants CSD2007-00023 and SAF2008-00611, and a grant from Fundación Ramón Areces. JV holds a fellowship from the Generalitat Valenciana and JLA a Juan de la Cierva contract supported by the Spanish Ministry of Science and Innovation.

Financial Disclosures

No conflict of interest is declared.

References

Alarcon, J. M., et al., 2004. Chromatin acetylation, memory, and LTP are impaired in CBP+/- mice: a model for the cognitive deficit in Rubinstein-Taybi syndrome and its amelioration. Neuron. 42**,** 947-59.

Barco, A., 2007. The Rubinstein-Taybi syndrome: modeling mental impairment in the mouse. Genes Brain Behav. 6 Suppl 1**,** 32-9.

Bartholdi, D., et al., 2007. Genetic heterogeneity in Rubinstein-Taybi syndrome: delineation of the phenotype of the first patients carrying mutations in EP300. J Med Genet. 44**,** 327-33.

Bentivegna, A., et al., 2006. Rubinstein-Taybi Syndrome: spectrum of CREBBP mutations in Italian patients. BMC Med Genet. 7**,** 77.

Bourtchouladze, R., et al., 2003. A mouse model of Rubinstein-Taybi syndrome: Defective long-term memory is ameliorated by inhibitors of phosphodiesterase 4. Proc Natl Acad Sci U S A. 100**,** 10518-22.

Chan, H. M., La Thangue, N. B., 2001. p300/CBP proteins: HATs for transcriptional bridges and scaffolds. J Cell Sci. 114**,** 2363-73.

Foley, P., et al., 2009. Further case of Rubinstein-Taybi syndrome due to a deletion in EP300. Am J Med Genet A.

Hennekam, R. C., et al., 1992. Psychological and speech studies in Rubinstein-Taybi syndrome. Am J Ment Retard. 96**,** 645-60.

Irwin, S., 1968. Comprehensive observational assessment: Ia. A systematic, quantitative procedure for assessing the behavioral and physiologic state of the mouse. Psychopharmacologia. 13**,** 222-57.

Kalkhoven, E., 2004. CBP and p300: HATs for different occasions. Biochem Pharmacol. 68**,** 1145-55.

Kasper, L. H., et al., 2006. Conditional knockout mice reveal distinct functions for the global transcriptional coactivators CBP and p300 in T-cell development. Mol Cell Biol. 26**,** 789-809.

Korzus, E., et al., 2004. CBP histone acetyltransferase activity is a critical component of memory consolidation. Neuron. 42**,** 961-72.

Levitas, A. S., Reid, C. S., 1998. Rubinstein-Taybi syndrome and psychiatric disorders. J Intellect Disabil Res. 42 (Pt 4)**,** 284-92.

Lopez de Armentia, M., et al., 2007. cAMP response element-binding protein-mediated gene expression increases the intrinsic excitability of CA1 pyramidal neurons. J Neurosci. 27**,** 13909-18.

Ogryzko, V. V., et al., 1996. The transcriptional coactivators p300 and CBP are histone acetyltransferases. Cell. 87**,** 953-9.

Oliveira, A. M., et al., 2006. Differential Role for CBP and p300 CREB-Binding Domain in Motor Skill Learning. Behav Neurosci. 120**,** 724-9.

Oliveira, A. M., et al., 2007. Transgenic mice expressing an inhibitory truncated form of p300 exhibit long-term memory deficits. Learn Mem. 14**,** 564-72.

Petrij, F., et al., 1995. Rubinstein-Taybi syndrome caused by mutations in the transcriptional co-activator CBP. Nature. 376**,** 348-51.

Phan, H. M., et al., 2005. GCN5 and p300 share essential functions during early embryogenesis. Dev Dyn. 233**,** 1337-47.

Roelfsema, J. H., Peters, D. J., 2007. Rubinstein-Taybi syndrome: clinical and molecular overview. Expert Rev Mol Med. 9**,** 1-16.

Roelfsema, J. H., et al., 2005. Genetic heterogeneity in Rubinstein-Taybi syndrome: mutations in both the CBP and EP300 genes cause disease. Am J Hum Genet. 76**,** 572-80.

Rogers, D. C., et al., 1997. Behavioral and functional analysis of mouse phenotype: SHIRPA, a proposed protocol for comprehensive phenotype assessment. Mamm Genome. 8**,** 711-3.

Roth, J. F., et al., 2003. Differential role of p300 and CBP acetyltransferase during myogenesis: p300 acts upstream of MyoD and Myf5. Embo J. 22**,** 5186-96.

Rubinstein, J. H., Taybi, H., 1963. Broad thumbs and toes and facial abnormalities. A possible mental retardation syndrome. Am J Dis Child. 105**,** 588-608.

Tanaka, Y., et al., 1997. Abnormal skeletal patterning in embryos lacking a single Cbp allele: a partial similarity with Rubinstein-Taybi syndrome. Proc Natl Acad Sci U S A. 94**,** 10215-20.

Viosca, J., et al., 2008. Germ line expression of H-RasG12V causes neurological deficits associated to Costello syndrome. Genes Brain Behav. Sep 22 [Epub ahead of print].

Wood, M. A., et al., 2006. A transcription factor-binding domain of the coactivator CBP is essential for long-term memory and the expression of specific target genes. Learn Mem. 13**,** 609-17.

Wood, M. A., et al., 2005. Transgenic mice expressing a truncated form of CREB-binding protein (CBP) exhibit deficits in hippocampal synaptic plasticity and memory storage. Learn Mem. 12**,** 111-9.

Yao, T. P., et al., 1998. Gene dosage-dependent embryonic development and proliferation defects in mice lacking the transcriptional integrator p300. Cell. 93**,** 361-72.

Zimmermann, N., et al., 2007. Confirmation of EP300 gene mutations as a rare cause of Rubinstein-Taybi syndrome. Eur J Hum Genet. 15**,** 837-42.

Figure legends

Figure 1. Facial dysmorphia and growth retardation in mice with reduced HAT activity. A. Top view of the head of *p300*$^{+/-}$, *cbp*$^{+/-}$ and control mice. All the *cbp*$^{+/-}$ mice (20 out of 20) and most of the *p300*$^{+/-}$ mice analyzed exhibited a blunt nose (8 out of 13 in a pure C57BL/6J background and 18 out of 24 in a DBA/C57 mixed background). The strongest dysmorphia was observed in *cbp*$^{+/-}$ mice and in some *p300*$^{+/-}$ mice in a pure genetic background. **B.** Computerized tomography analysis of p300 (left) and CBP (right) deficient mice skulls. Sagittal sections from mutant (red) and control littermates (white) were overlapped and aligned for comparison. *Cbp*$^{+/-}$ (3 out of 3) and, at lesser extent, *p300*$^{+/-}$ mice in a pure C57BL/6J background (2 out of 3) showed depressed anterior frontal bone and shortened and depressed nasal bridge (blue arrows). We did not observe clear differences in the alignment of *p300*$^{+/-}$ mice and control littermates in a DBA/C57 background (3 out of 3, not shown). **C-D**. Reduced weight and body length of adult *p300*$^{+/-}$ mice in a pure C57BL/6J background (C) and a mixed DBA/C57 background (D). (*) indicates significant differences between genotypes.

Figure 2. Normal gross brain anatomy in p300 deficient mice. A. Nissl staining of coronal brain sections from *p300*$^{+/-}$ (bottom) in a pure C57BL/6J background and wild-type littermates (top). No apparent morphological defects were detected in brains from mutant mice (scale bar=1 mm). **B-C**. MAP2 (B) and Synaptophysin (C) inmunostaining of adult *p300*$^{+/-}$ and control mice brain sections. Cytoarchitecture of hippocampus, cortex, amygdala and cerebellum (from top to bottom) were similar between mutant and wild-type mice (scale bar=200 μm).

Figure 3. Locomotor activity and anxiety in p300 deficient mice. A. *p300*$^{+/-}$ mice in a pure C57BL/6J background showed lower pelvic elevation during ambulation. (n=11 wt and 10 *p300*$^{+/-}$). **B.** Rotarod performance of *p300*$^{+/-}$ mice was normal (n=5 wt and 8 *p300*$^{+/-}$). **C-D.** Open field activity. *p300*$^{+/-}$ mice (n=11) and control littermates (n=10) travelled similar distances (C) and spent the same time in the central area of the arena (D). **E-F**. In the elevated plus maze (11 mutant and 9 wild-type mice), *p300*$^{+/-}$ mice showed reduced arm entries (E) and spent less time in the open arms (F). (*) indicates significant differences between genotypes.

Figure 4. Cognitive abilities in p300 deficient mice. A. *p300*$^{+/-}$ mice in a pure C57BL/6J background showed normal long-term memory for object recognition 24h after training (n=8 for each genotype). **B-G.** Spatial learning and memory in the water maze (*p300*$^{+/-}$ mice: dark squares, n=10; wild type littermates: open circles, n=11). **B**. Both genotypes learned similarly in the visible and hidden platform tasks, but mutant mice showed significant impairments in the transfer task. **C.** *p300*$^{+/-}$ mice showed enhanced thigmotaxis in the water maze during the first days of training in the visible platform task. **D**. *p300*$^{+/-}$ mice showed reduced swimming speed in the water maze. **E.** Probe trials were performed on days H5 (P1) and H9 (P2) of training in the hidden platform task. No significant differences were observed in the two probe trials. **F**. In the transfer task, mutant mice explored more than wild-type littermates the quadrant were the platform was located during the hidden platform task. **G.** A third probe trial (P3) was performed 24 h after T5. No significant difference was observed. **H.** Contextual and cued fear conditioning is similar in *p300*$^{+/-}$ (n=10) and wild-type (n=11) mice. (*) indicates significant differences between genotypes.

Figure 5. Bulk neuronal histone acetylation in p300 deficient mice. A. Western-blot of hippocampal protein extracts from *p300*$^{+/-}$ in a pure C57BL/6J background and control (wt) mice using α-β-actin, α-H2B (non acetylated), α-AcH2B, α-AcH2A, α-AcH3 and α-AcH4 antibodies (two left lanes). We analyzed in parallel samples from mice injected with sodium butyrate (NaBt) or vehicle (PBS) as a positive control (two central lanes). Western-blot of hippocampal protein extracts from *cbp*$^{+/-}$ and control (wt) mice using the same antibodies (two right lanes). **B.** Quantification of western-blot results. No significant differences were found in the level of acetylation of hippocampal histones in *p300*$^{+/-}$ mice (upper panel, n=3 for both genotypes). However, the quantification of western-blot results confirmed the specific deficit in acetylation of bulk histone H2B in the hippocampus of *cbp*$^{+/-}$ mice (lower panel, n=4 for both genotypes). **C.** Images of the cellular layer in the CA1 subfield of *p300*$^{+/-}$ mice and control littermates. Sagittal brain sections were immunostained with antibodies against acetylated forms of histones H2A, H2B, H3 and H4. The levels of histone acetylation were similar in both genotypes. As a control, we also present the staining of sections from wild type mice injected with the HDACi sodium butyrate or with vehicle (scale bar=100 μm).

Figure 6. Quantitative RT-PCR analysis of candidate genes revealed in the microarray screen. Total RNA was isolated from the hippocampi of *p300*$^{+/-}$ mice and control littermates (n=4-5 per genotype). The following genes were assessed (from left to right): *txnip* (thioredoxin interacting protein, p=0.484); *anxa4* (annexin A4, p=0.512); *tspYl1* (testis-specific protein Y-encoded-like 1, p=0.253); *vamp3* (vesicle-associated membrane protein 3, p=0.849); the RIKEN cDNA *1190005F20Rik* (p=0.358); *pank3* (pantothenate kinase 3, p=0.968) and *Ep300* (E1A binding protein p300, p<0.001).

Transcripts for *crebbp* (CREB binding protein, p=0.613) and histone cluster 1c (*hist1h1c*, p=0.640) were also assessed as controls. This analysis only revealed a significant reduction in the level of p300 mRNA. (*) indicates significant differences between genotypes.

Table 1: Viability of *p300*$^{+/-}$ mice in a pure C57BL/6J and in a mixed C57/DBA genetic background

	wild type	*p300* $^{+/-}$	*P*
C57BL/6J	80 (78.4%)	22 (21.6%)	<0.001
C57/DBA	57 (54.3%)	48 (45.7%)	0.581

For each genetic background, number and percentage of individuals obtained from wild-type x heterozygote crosses are shown. The percentage of mutant mice was compared with same-sized samples following a mendelian distribution using Fisher's Exact tests.

Table 2. Neurological characterization of *p300*$^{+/-}$ mice

	Wild type (n=11)	*p300*$^{+/-}$ (n=10)	*P*
Spontaneous activity	2 (2-2)	2 (2-2)	1.00
Locomotor activity	18 ± 1	16 ± 1	0.16
Gait	0 (0-0)	0 (0-0)	1.00
Palpebral closure	0 (0-0)	0 (0-0)	1.00
Skin colour	1 (1-1)	1 (1-1)	0.16
Daefecation	3 (2-4)	1.5 (1- 5.2)	0.25
Tail elevation	2 (1-2)	1 (1-1.2)	0.05
Pelvic elevation	3 (3-3)	2 (2-3)	**0.02***
Limb grasping	1 (1-1)	1 (1-1)	0.16
Grip strength	3 (2-3)	3 (3-3)	0.08
Negative geotaxis	0 (0-0)	0 (0-0)	1.00
Touch escape	3 (3-3)	2 (2-3)	0.05
Irritability	1 (1-1)	1 (1-1)	1.00
Lacrimation	0 (0-0)	0 (0-0)	0.29
Wire manoeuvre	2 (2-2)	2 (2-3)	0.65
Fear	0 (0-0)	0 (0-0)	1.00
Provoked biting	0.5 (0-1)	1 (0.5-1)	0.24
Piloerection	0 (0-0)	0 (0-0)	1.00
Body position	3 (3-3)	3 (3-3)	0.34
Visual placing	2 (2-3)	3 (2-3)	0.18
Transfer arousal	4 (4-5)	4 (4-5)	0.89
Corneal reflex	1 (1-1)	1 (1-1)	1.00
Righting reflex	0 (0-0)	0 (0-0)	1.00
Contact righting réflex	1 (1-1)	1 (1-1)	1.00
Pineal reflex	1 (1-1)	1 (1-1)	1.00
Toe pinch	3 (2-3)	2 (2-2.5)	**0.02***
Trunk curl	0 (0-0)	0 (0-0)	1.00
Tremor	0 (0-1)	0 (0-0.2)	0.70
Abdominal tone	1 (1-1)	1 (1-1)	1.00
Limb tone	1 (1-1)	1 (1-1)	0.29
Urination	0 (0-1)	0 (0-0)	**0.04***
Vibrissae	0 (0-1)	0 (0-0.2)	0.70
Vocalisation	1 (1-1)	1 (1-1)	1.00

Data are expressed as either mean ± SEM or median followed by the interquartile range in parenthesis. P-values are calculated using t-test for data expressed as mean ± SEM or Mann-Whitney test for data expressed as median followed by the interquartile range.

Table 3. Mutations in EP300 locus in humans and mice

	Mutation	Protein	Reference
RTST patients			
Patient 1	Point mutation in exon 10 generating a Stop codon	* R648X	(Bartholdi et al. 2007)
Patient 2	Deletion in exon 20	Q1209fsX1226	(Bartholdi et al. 2007)
Patient 3	Microdeletion (8pb) in exon 15	S959fsX966	(Bartholdi et al. 2007)
Patient 4	Deletion stretching from promoter to first intron	* No protein	(Bartholdi et al. 2007)
Patient 5	Microdeletion (1pb) in exon 31	P2366fsX2401	(Zimmermann et al. 2007)
Patient 6	Deletion of exons 3-8	* K243Xfs271	(Foley et al. 2009)
Mouse strains			
$p300^{+/-}$	Deletion stretching from exon 4 to 6	* ~aa330fsX	(Yao et al. 1998; this study)
p300Δ1	Truncated cDNA (Exons 1-16) under CaMKII promoter	S1032X	(Oliveira et al. 2007)
$p300^{KIX/KIX}$	Triple point mutation in the KIX domain (exon 10) in homozygosis	Y630A, A634N, Y638A	(Oliveira et al 2006)

* Mutations leading to the production of no protein or short truncated proteins (<30% of full length).

Figure 1

Click here to download high resolution image

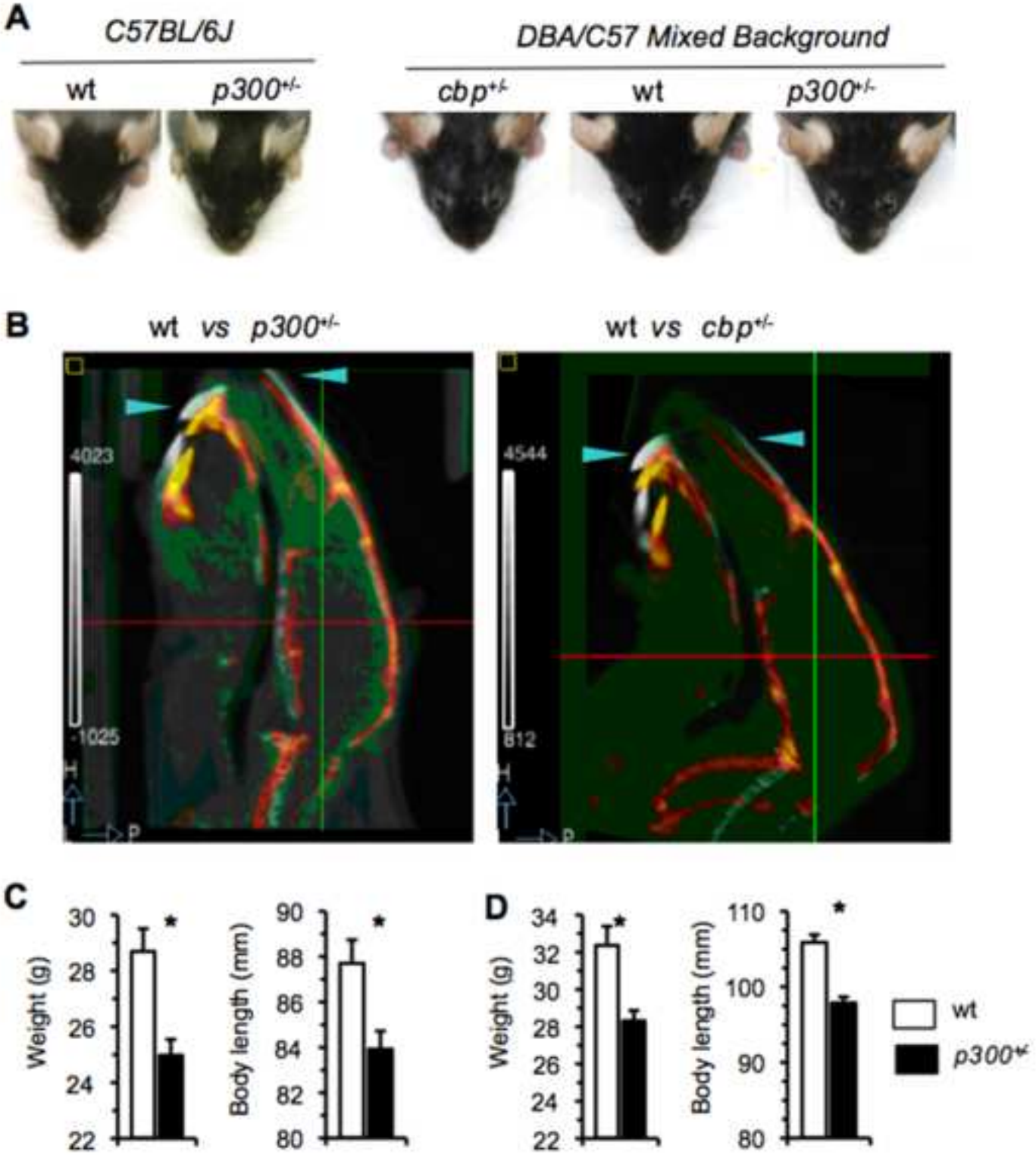

Figure 2

Click here to download high resolution image

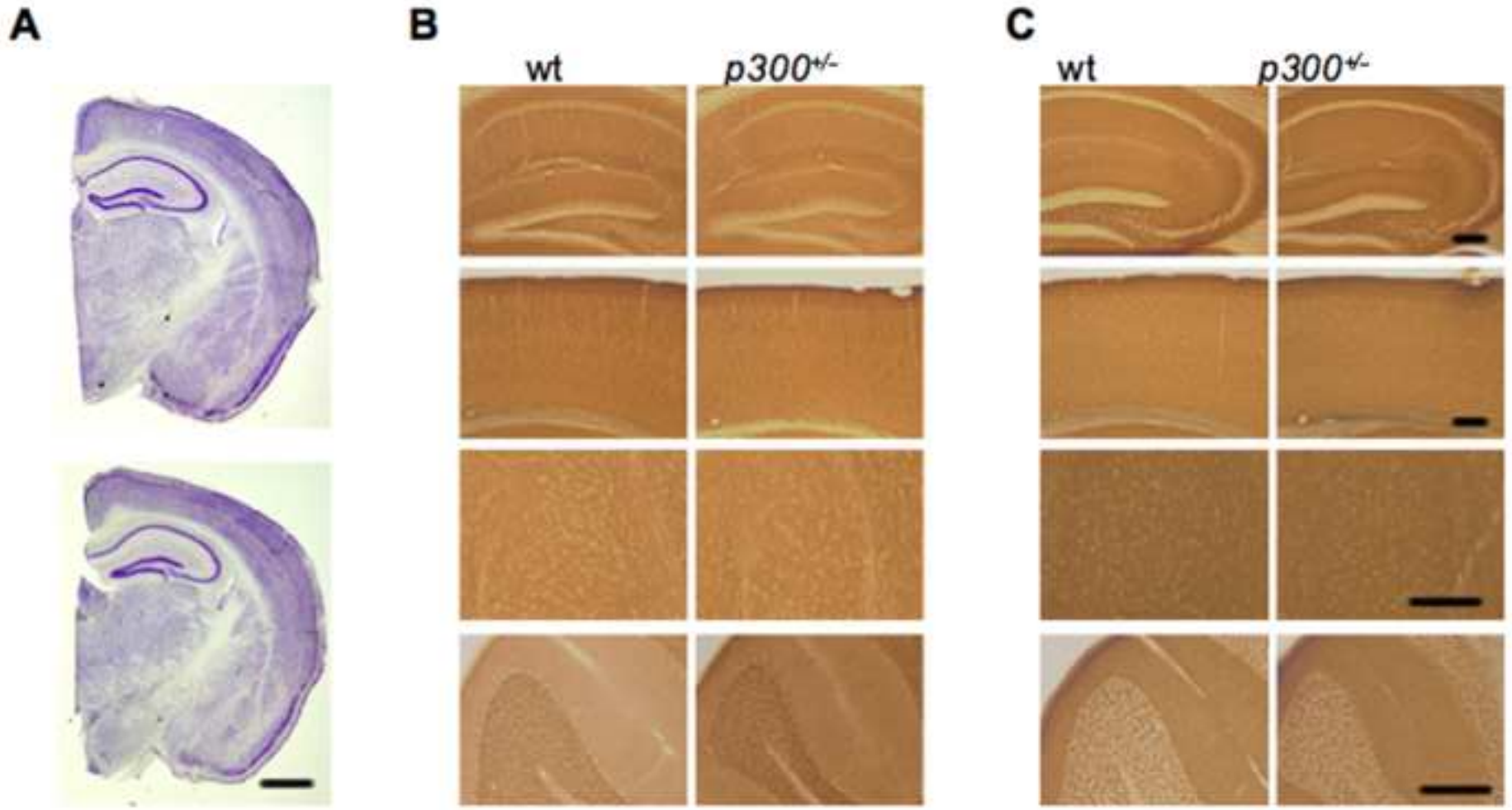

Figure 3

Click here to download high resolution image

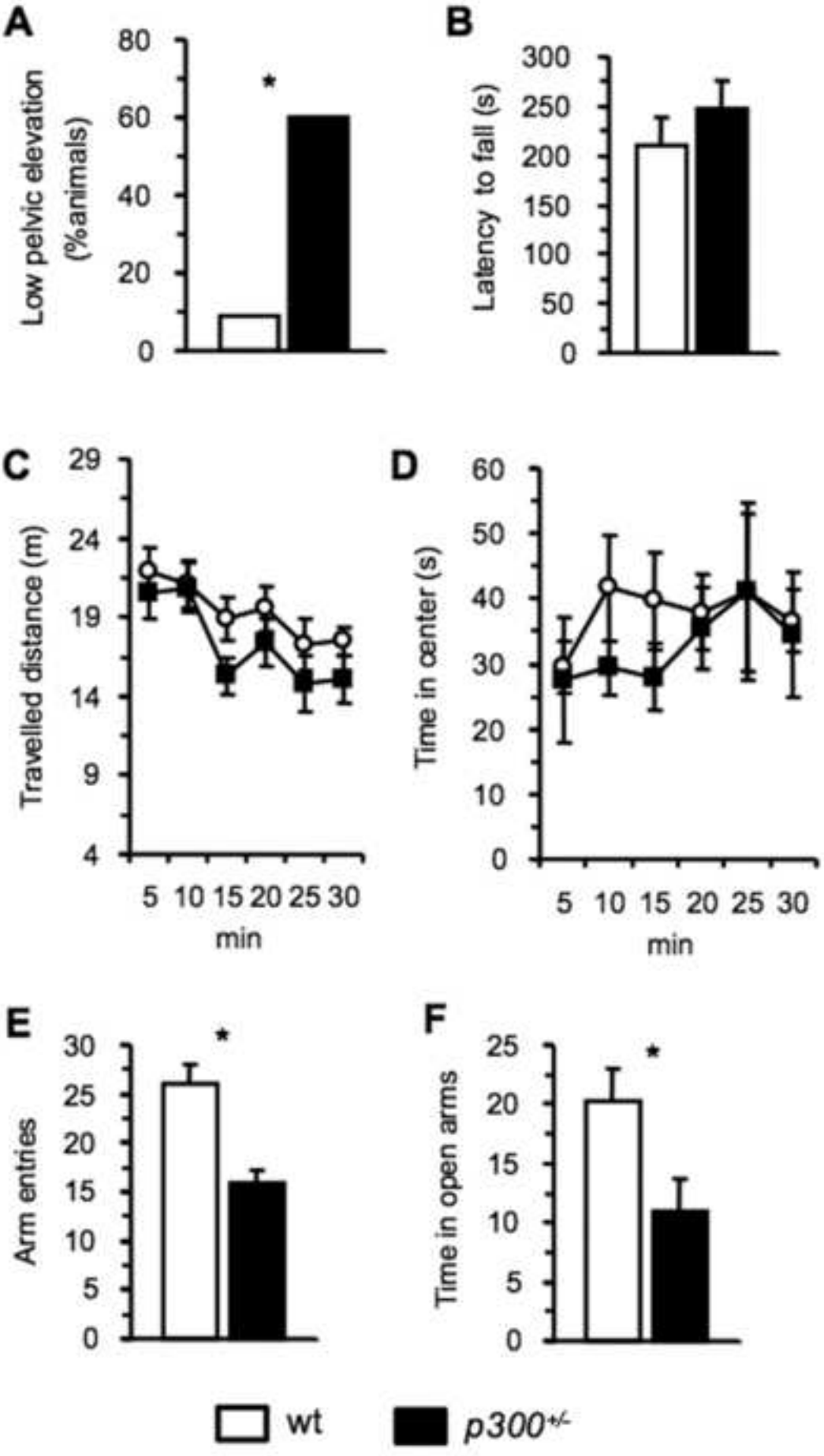

Figure 4

Click here to download high resolution image

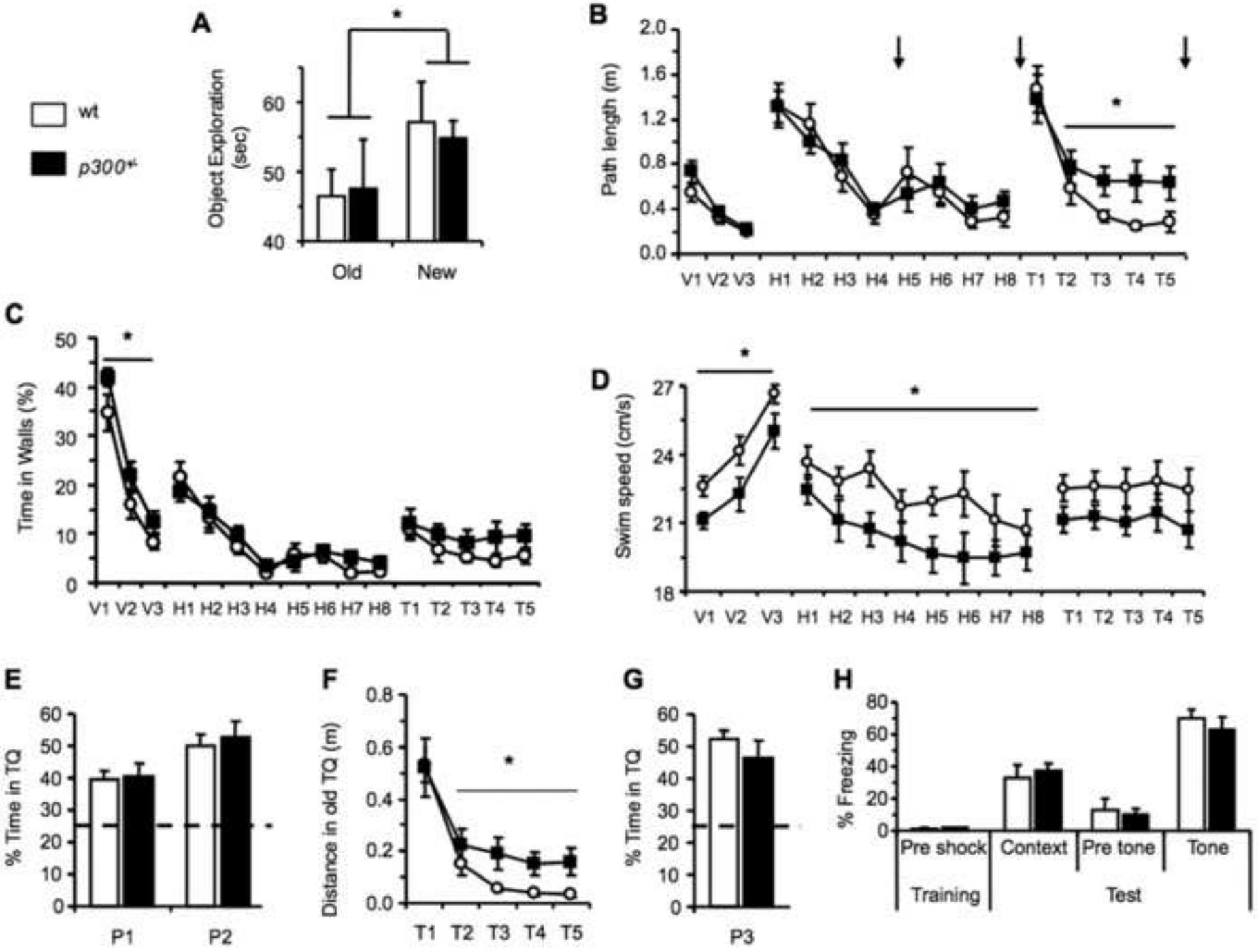

Figure 5

Click here to download high resolution image

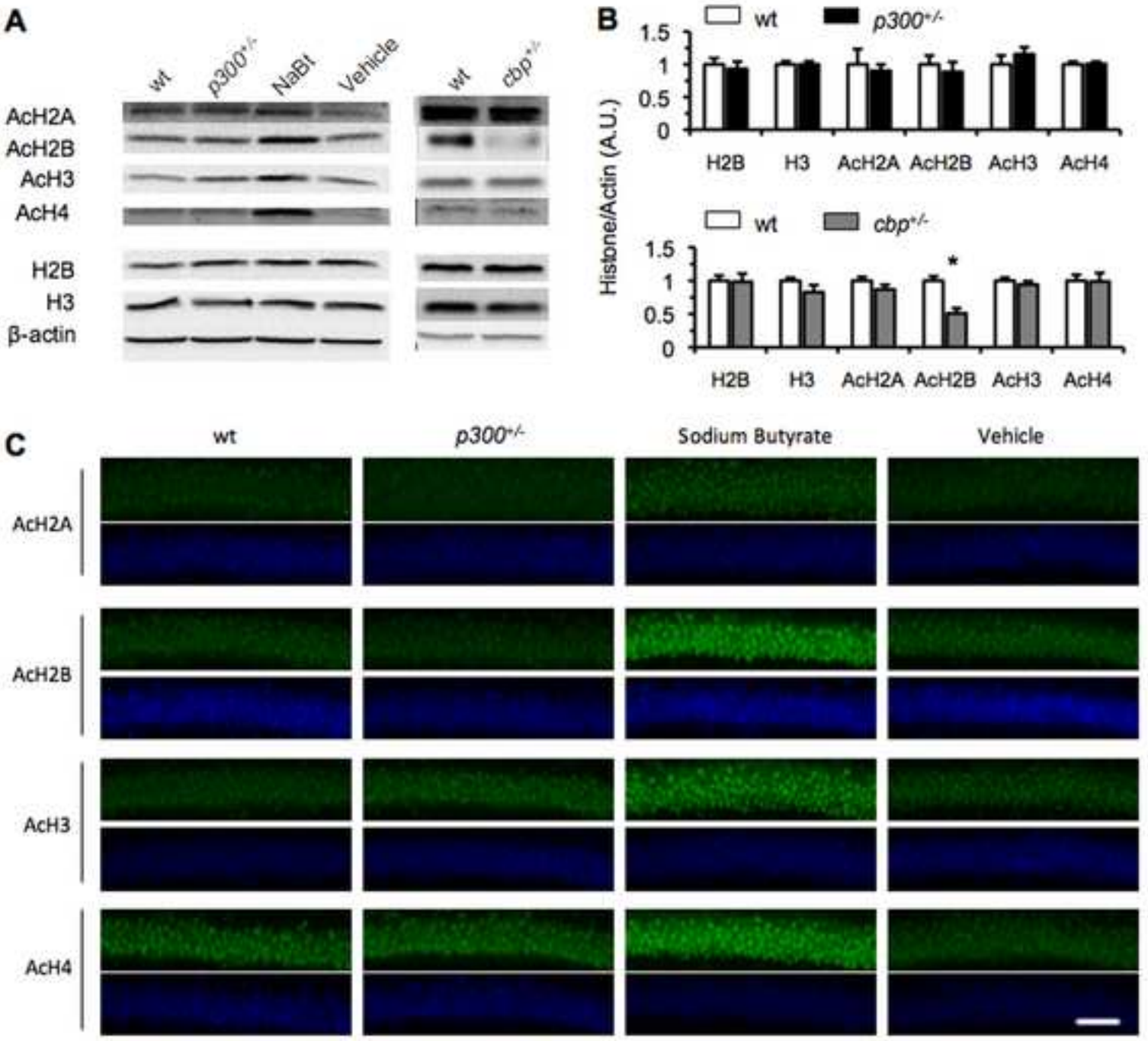

Figure 6

Click here to download high resolution image

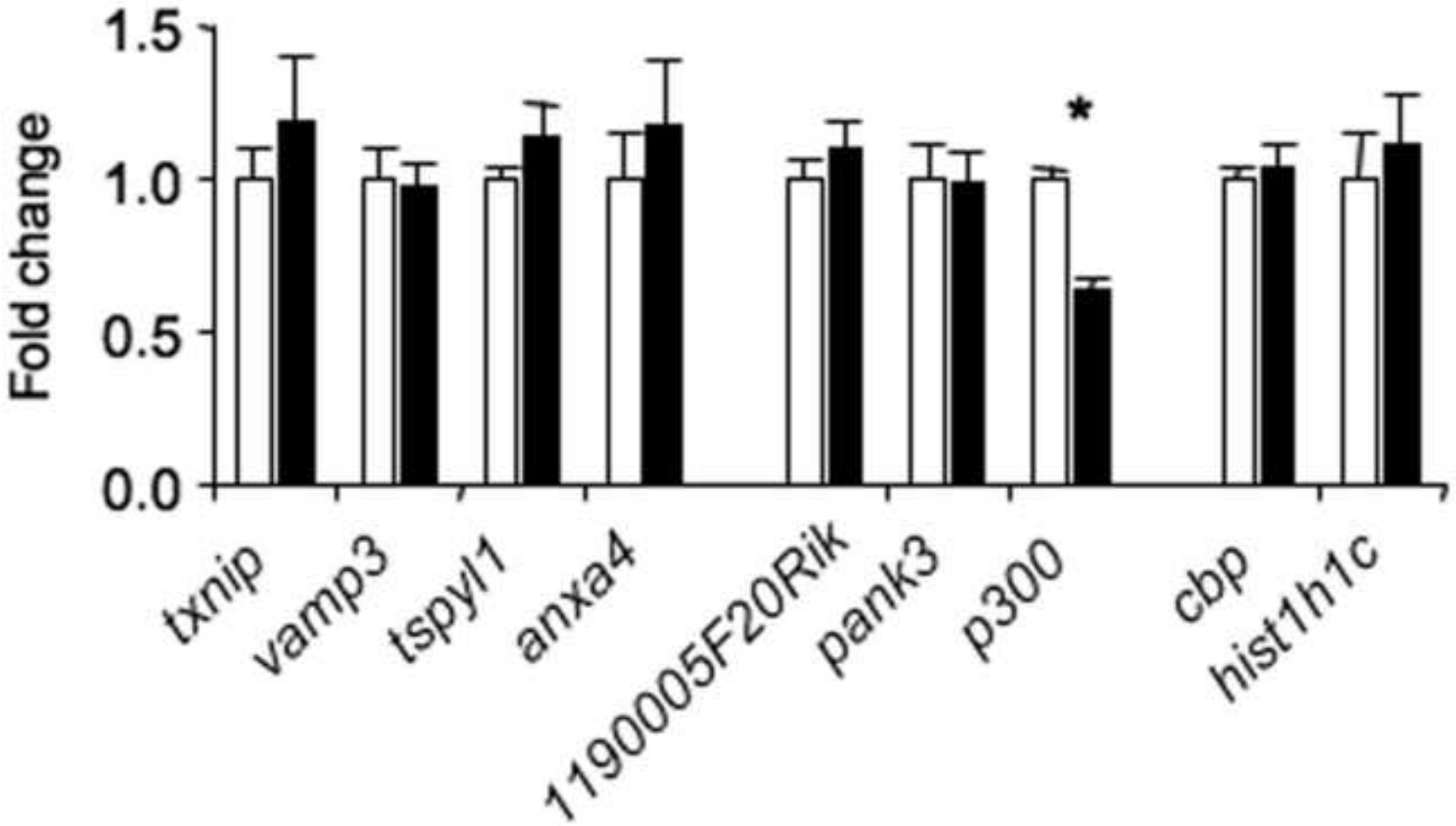

6-Supplementary Material

Click here to download 6-Supplementary Material: SUPPLEMENTAL MATERIAL.pdf